Perturbed hematopoiesis in mice lacking ATMIN

Fernando Anjos-Afonso[1,5], Joanna I. Loizou[2,6], Nnennaya Kanu[2,7], Sukhveer Purewal[3], Dominique Bonnet[1*] and Axel Behrens[2,4*]

1-Haematopoietic Stem Cell Lab, The Francis Crick Institute, Lincoln's Inn Fields Laboratory, 44 Lincoln's Inn Fields, London WC2A 3LY, UK.
2-Mammalian Genetics Lab, The Francis Crick Institute, Lincoln's Inn Fields Laboratory, 44 Lincoln's Inn Fields, London WC2A 3LY, UK.
3-Flow Cytometry Lab, The Francis Crick Institute, Lincoln's Inn Fields Laboratory, 44 Lincoln's Inn Fields, London WC2A 3LY, UK.
4-School of Medicine, King's College London, Guy's Campus, London SE1 1UL, UK.
5-Current address: Haematopoietic Signalling Group, European Cancer Stem Cell Research Institute, Cardiff University, Hadyn Ellis Building, Maindy Road, Cardiff CF24 4HQ.
6-Current address: CeMM Research Center for Molecular Medicine of the Austrian Academy of Sciences, Lazarettgasse 14, AKH BT 25.3, 1090 Vienna, Austria.
7-Current address: Translational Cancer Therapeutics Laboratory, UCL Cancer Institute, Paul O'Gorman Building, University College London, 72 Huntley Street, London WC1E 6DD, UK.

*To whom correspondence should be addressed:
Tel.: 44-207-269-3361; Fax: 44-207-269-3581; E-mail: axel.behrens@crick.ac.uk
Or
Tel: +44 (0) 20 7269 3282; Fax: +44 (0) 20 7269 3581; Email: dominique.bonnet@cancer.org.uk

Short title: Perturbed hematopoiesis in mice lacking ATMIN
Text word count: 1216 excluding Abstract, Figure Legends and References
Abstract word count: 198
Number of figures: 2
Number of references: 14
Scientific category: Hematopoiesis and stem cells (Brief Report)

Key points:

- ATMIN deletion using Vav-Cre causes chronic leukopenia, with fewer B cells and common myeloid progenitors
- Long-term hematopoietic stem cells in ATMIN-deficient mice show increased cell cycling and are more prone to exhaustion under stress

Abstract

The ATM-interacting protein ATMIN mediates non-canonical ATM signaling in response to oxidative and replicative stress conditions. Like ATM, ATMIN can function as a tumor suppressor in the hematopoietic system: deletion of *Atmin* under the control of CD19-Cre results in B cell lymphomas in aging mice. ATM signaling is essential for lymphopoiesis and hematopoietic stem cell (HSC) function; however, little is known about the role of ATMIN in hematopoiesis. We thus sought to investigate if the absence of ATMIN would affect primitive hematopoietic cells in an ATM-dependent or -independent manner. Apart from its role in B cell development, we show that ATMIN has an ATM-independent function in the common myeloid progenitors (CMPs) when *Atmin* is deleted in the entire hematopoietic system using Vav-Cre. Despite the lack of lymphoma formation, the chronic leukopenia in ATMIN-deficient mice, as a result of high levels of apoptosis in B cells and CMPs and induced a compensatory mechanism in which HSCs displayed enhanced cycling. Consequently, ATMIN-deficient HSCs showed impaired regeneration ability, especially when aged with the induction of the DNA oxidative stress response. ATMIN therefore has multiple roles in different cell types and its absence results in perturbed hematopoiesis, especially during stress conditions and aging.

Introduction

ATM (ataxia telangiectasia mutated) coordinates cell-cycle checkpoints with DNA repair in response to DNA damage[1]. ATM can be activated by the MRN complex (MRE11/RAD50/NBS1) via interaction with NBS1[2] but can also be activated by the ATM interactor ATMIN[3]. ATMIN has a complementary function to NBS1: ATMIN is dispensable for ionizing radiation-induced ATM signaling, whereas NBS1 is dispensable for ATM activation following ionizing damage or hypotonic stress[3,4].

ATMIN has been shown to function in conditions of oxidative stress and aging[5] and also as a transcription factor[6]. We have previously shown that ATMIN-deleted B cells (induced by CD19-Cre) have impaired class switch recombination and increased genomic instability, leading to B cell lymphomas[7]. In contrast, mice conditionally deleted of *Atmin* using Mx1-Cre developed B cell lymphopenia[8]. It is unclear whether the lack of B cell lymphoma formation in this mouse model is due to a B cell developmental defect or to other deficiencies in primitive hematopoietic cells that prevent the accumulation of genetically unstable cells. Since the role of ATMIN in hematopoietic stem/progenitor cells is currently unknown, we sought to investigate a possible role for ATMIN in primitive hematopoietic cells and whether this would be ATM-dependent or -independent.

Materials and Methods

Vav-Atmin$^{\Delta/\Delta}$ mice

Atmin$^{f/f}$ mice (described previously[5,7]) were crossed with heterozygous Vav-Cre mice to generate Vav-*Atmin*$^{\Delta/\Delta}$ mice. Gene deletion efficiency and genotyping was determined using a PCR-based assay using primers specific for the floxed exon 4, deleted exon 4 and WT *Atmin* alleles as well as for Vav-Cre (See Table S1).

Intracellular immunostaining

As briefly described[9], cells were incubated with antibodies against extracellular antigens, then fixed in PBS with 2% methanol-free formaldehyde at room temperature (RT) (for Ki-67; BD Biosciences) or at 37°C (for pKap1; Bethyl Laboratories and Bim; Cell Signaling) for 10 min. Cells were then permeabilized with PBS containing 0.1% Triton-X-100 (Sigma) for 10 min at RT, blocked using PBS containing 5% serum for 15 min and incubated with primary antibodies at 4°C for 1 hour, followed by appropriate secondary antibodies in the same conditions. Cells were resuspended with PBS/2% FBS containing DAPI and pulse processing was used to exclude any unstained, apoptotic and clumped cells.

Please see Supplementary Information for more detailed Methods.

Results and discussion

Vav1 promoter-mediated deletion of *Atmin* exon 4 generates a null allele (Vav-*Atmin*$^{\Delta/\Delta}$) in the hematopoietic system (Figures S1A and S1B).

ATMIN-deficient mice were born healthy and were not anemic but were leukopenic at 8-12 weeks (Figure S1C-D). Unlike the CD19-Cre model[7], mice did not develop lymphoma, and instead numbers of B cells were reduced (Figure S2A-F). The numbers of splenic B cells was dramatically reduced (Figure S2A, B) and resulted in a complete absence of germinal centers (GC) (Figure S2C). B cell apoptosis was increased, and while oxidative stress was unaffected there was a pronounced reduction in *Dynll1* expression, as previously described[8] (Figure S2D-F). The pronounced B cell lymphopenia in the Mx-Cre model[8] and the Vav-*Atmin*$^{\Delta/\Delta}$ mice described here are in contrast to the CD19-Cre model[7], which have normal B cell numbers. The reduction of splenic GC B cells may explain the absence of lymphoma development in the Mx-Cre model[8] and the Vav-*Atmin*$^{\Delta/\Delta}$ mice. ATMIN-deficient B cells displayed a significant increase in the DNA damage response, consistent with an ATM-dependent competitive function of ATMIN[4,7] (Figure S2G-H). Numbers of pre-B cells in the bone marrow (BM) were also significantly lower (Figure S2I-K). These data suggested an early developmental defect that does not allow the accumulation of damaged B cells. We thus analyzed the primitive hematopoietic cell compartment in more detail.

In young ATMIN-deficient mice (8-12 weeks), a ~40% reduction in BM cellularity was observed across all cell types, with a reduced frequency of common myeloid progenitors (CMPs) (Figure 1A-B). Sub-populations upstream of CMPs, particularly LT-HSCs, showed more cells that had exited quiescence (Figure 1C), supported by reduced expression of *Cdkn1c* (*p57*^{Kip2}) in the different primitive cell sub-types and *Rbl2* (p130) in LT-HSCs (Figure S3A). Increased LT-HSC cycling to compensate for the reduced B cell and

CMP compartments in Vav-*Atmin*$^{\Delta/\Delta}$ mice could potentially affect LT-HSC function. Indeed, the regenerative capacity of Vav-*Atmin*$^{\Delta/\Delta}$ LT-HSCs 16 weeks post-transplantation was reduced 16-fold compared with control cells, affecting all three lineages (Figures 1D and S3B-C). Importantly, ATMIN-deficient LT-HSCs were mostly unable to regenerate hematopoiesis when re-transplanted (Figure 1D). Vav-*Atmin*$^{\Delta/\Delta}$ mice succumbed to multiple doses of the myeloid-suppressive agent 5-FU (5-fluorouracil) faster than *Atmin*$^{f/f}$ mice (Figure S3D). Despite the apparent lack of oxidative stress and DNA damage in young Vav-*Atmin*$^{\Delta/\Delta}$ cells at steady state (Figure 1E-G), these results suggest that stresses induced during regeneration disturbed LT-HSC function.

Aged (55-65-week-old) Vav-*Atmin*$^{\Delta/\Delta}$ mice continued to have reduced BM cellularity (Figure 1H) and no incidence of lymphoma. We observed similar defects in aged ATMIN-deficient B cells as reported[7] (data not shown) and also a reduced CMP compartment (Figure 1I). Although numbers of short-term (ST)-HSCs and multipotent progenitors (MPPs) were not altered in aged ATMIN-deficient mice, the proportion of these sub-populations was mildly increased, perhaps because they cycled more in younger but not in aged mice (Figure 1H-J). Again, when aged LT-HSCs were transplanted, ATMIN-deficient cells were unable to provide long-term reconstitution (Figure 1K). There were no apparent signs of senescence (such as increased *p16*^{Ink4a} and *p19*^{Arf} expression) in any of the aged ATMIN-deficient primitive sub-populations (data not shown) and no increase in ROS production in ATMIN-deficient LT-HSCs was observed (Figure 1L), unlike *Atm*$^{-/-}$ mice[10,11]. However, in contrast with young cells, we observed a significant increase in DNA oxidation repair gene expression in aged ATMIN-deficient LT-HSCs, and

pKap1 expression was upregulated, suggesting increased DNA damage in these cells (Figure 1M-N).

Next, we went on to investigate the function of ATMIN in the CMP compartment. The very modest oxidative stress detected in the myeloid progenitors did not seem to play an evident role in reducing this cellular fraction in ATMIN-deficient mice (Figure 2A-C). We also observed neither increased DNA damage (Figure 2D-E) nor evidence of developmental defects (Figure 2F) in Vav-*Atmin*$^{\Delta/\Delta}$ CMPs compared with control cells. However, a significant increase in late apoptosis was detected in Vav-*Atmin*$^{\Delta/\Delta}$ CMPs (Figure 2G) but not in other primitive compartments (not shown) and this was accompanied by a ~33-fold decrease in *Dynll1* expression (a direct transcriptional target of ATMIN[6], Figure 2H). Immunofluorescent studies revealed significant co-staining of Bim with MitoTracker dye in Vav-*Atmin*$^{\Delta/\Delta}$ cells (Figure 2I-K). This observation is consistent with the decrease in Dynll1 levels freeing Bim to be translocated into mitochondria, triggering higher apoptosis[11] in Vav-*Atmin*$^{\Delta/\Delta}$ CMPs.

We reveal ATMIN as a novel player with multiple functions in hematopoiesis, both ATM-dependent and -independent. Apart from its roles in B cell development[7,8], we have uncovered an important ATM-independent function of ATMIN in the CMP compartment. ATMIN-deficient mice also have impaired LT-HSC function during regeneration and aging, most likely due to exhaustion from compensating the reduced/damaged lymphoid and myeloid compartments over time. It would be interesting to dissect other possible roles that ATMIN might have in myeloid development with more specific lineage

gene deletion approaches, as myeloid cells can differentiate without passing the CMP stage[13-15]. Interestingly, *ATMIN* is overexpressed in inv16 acute myeloid leukemias (AMLs) compared with normal myeloid cells[16], and is located on chromosome 16 where rearrangements are common in AML. ATMIN may therefore also have a role in myeloid neoplasms.

Acknowledgments

This work was supported by The Francis Crick Institute/Cancer Research UK core funding to AB and DB. This work was also supported by an ERC grant (281661 ATMINDDR) to A.B. We thank the Biological Resources Unit and Flow Cytometry core facility for valuable technical help and Dr. Catherine Cremona for help with manuscript editing.

Author contributions

F.A-A: conceived, designed and performed experiments, and wrote the manuscript. J.I.L: provided mice, conceived, and performed some experiments. S.P. optimized, performed and analyzed data related to ImageStream experiments. N.K: provided mice and helped designing experiments; D.B. and A.B. conceived the study.

Conflict of interest

There is no conflict of interest to declare.

References

1-Shiloh Y, Ziv Y. The ATM protein kinase: regulating the cellular response to genotoxic stress, and more. Nat Rev Mol Cell Biol. 2013;14(4):197-210.

2-Uziel T, Lerenthal Y, Moyal L, Andegeko Y, Mittelman L, Shiloh Y. Requirement of the MRN complex for ATM activation by DNA damage. EMBO J. 2003;22(20):5612-5621.

3-Kanu N, Behrens A. ATMIN defines an NBS1-independent pathway of ATM signalling. EMBO J. 2007;26(12):2933-2941.

4-Zhang T, Penicud K, Bruhn C, et al. Competition between NBS1 and ATMIN controls ATM signaling pathway choice. Cell Rep. 2012;2(6):1498-1504.

5-Kanu N, Penicud K, Hristova M, et al. The ATM cofactor ATMIN protects against oxidative stress and accumulation of DNA damage in the aging brain. J Biol Chem. 2010;285(49):38534-38542.

6-Jurado S, Conlan LA, Baker EK, et al. ATM substrate Chk2-interacting Zn2+ finger (ASCIZ) Is a bi-functional transcriptional activator and feedback sensor in the regulation of dynein light chain (DYNLL1) expression. J Biol Chem. 2012;287(5):3156-3164.

7-Loizou JI, Sancho R, Kanu N, et al. ATMIN is required for maintenance of genomic stability and suppression of B cell lymphoma. Cancer Cell. 2011;19(5):587-600.

8-Jurado S, Gleeson K, O'Donnell K, et al. The Zinc-finger protein ASCIZ regulates B cell development via DYNLL1 and Bim. J Exp Med. 2012;209(9):1629-1639.

9-Anjos-Afonso F, Currie E, Palmer HG, Foster KE, Taussig DC, Bonnet D. CD34(-) cells at the apex of the human hematopoietic stem cell hierarchy have

distinctive cellular and molecular signatures. Cell Stem Cell. 2013;13(2):161-174.

10-Ito K, Hirao A, Arai F, et al. Regulation of oxidative stress by ATM is required for self-renewal of haematopoietic stem cells. Nature. 2004;431(7011):997-1002.

11-Ito K, Takubo K, Arai F, et al. Regulation of reactive oxygen species by Atm is essential for proper response to DNA double-strand breaks in lymphocytes. J Immunol. 2007;178(1):103-110.

12-Puthalakath H, Huang DC, O'Reilly LA, King SM, Strasser A. The proapoptotic activity of the Bcl-2 family member Bim is regulated by interaction with the dynein motor complex. Mol Cell. 1999;3(3):287-296.

13-Adolfsson J, Mansson R, Buza-Vidas N, et al. Identification of Flt3+ lympho-myeloid stem cells lacking erythro-megakaryocytic potential a revised road map for adult blood lineage commitment. Cell. 2005;121(2):295-306.

14-Arinobu Y, Mizuno S, Chong Y, et al. Reciprocal activation of GATA-1 and PU.1 marks initial specification of hematopoietic stem cells into myeloerythroid and myelolymphoid lineages. Cell Stem Cell. 2007;1(4):416-427.

15-Pronk CJ, Rossi DJ, Mansson R, et al. Elucidation of the phenotypic, functional, and molecular topography of a myeloerythroid progenitor cell hierarchy. Cell Stem Cell. 2007;1(4):428-442.

16- http://servers.binf.ku.dk/hemaexplorer/75432-29590613/data/stdout.html.

Figure legends

Figure 1. Vav-*Atmin*$^{\Delta/\Delta}$ LT-HSCs have impaired functions during regeneration and aging. Experiments were performed with young (**A**-**F**) and aged (**H**-**N**) BM cells. Black bars/symbols represent *Atmin*$^{f/f}$ and white Vav-*Atmin*$^{\Delta/\Delta}$ unless otherwise indicated. (**A**, **H**) Total cellularity and absolute numbers of the indicated sub-populations were determined in the BM of *Atmin*$^{f/f}$ and Vav-*Atmin*$^{\Delta/\Delta}$ mice (from two tibiae, two femurs and two iliac crests; n=5-6/genotype). (**B**, **I**) Frequencies of the different primitive BM stem/progenitor sub-populations (n=6-8/genotype) were also analyzed. Horizontal bars indicate the mean. (**C**, **J**) Cell cycle distribution was determined using Ki67/DAPI stains in the indicated BM stem/progenitor sub-populations (n=4/genotype). (**D**) To evaluate the regeneration capacity of LT-HSCs, peripheral blood (PB) chimerism was determined at different time points from sub-lethally irradiated NSG mice (non-obese diabetic/severe combined immunodeficiency disease/interleukin-2 receptor γ-chain–null; CD45.1 due to the mixed background) that were transplanted with 15 young LT-HSCs from either *Atmin*$^{f/f}$ or Vav-*Atmin*$^{\Delta/\Delta}$ mice (CD45.2). After 16 wks, 15 LT-HSCs were sorted by flow cytometry from primary mice and re-transplanted into separate secondary recipients and PB chimerism was determined at different time points. (**K**) PB chimerism was also determined from sub-lethally irradiated NSG mice transplanted with 15 aged LT-HSCs from either *Atmin*$^{f/f}$ or Vav-*Atmin*$^{\Delta/\Delta}$ mice. Each symbol indicates a mouse and horizontal lines represent median reconstitution levels. (**E**, **L**) As *Atm*$^{-/-}$ LT-HSCs have 10-fold elevated ROS compared to WT cells[10], we investigated ROS production in *Atmin*$^{f/f}$ or Vav-*Atmin*$^{\Delta/\Delta}$ LT-HSCs. DCFDA stains for ROS detection are shown. Values indicate the percentage of ROS-positive cells (n=3/genotype). (**F, M**) qRT-PCR for the expression of the indicated DNA oxidation repair genes in LT-HSCs was also evaluated. Expression values were relative to the mean of each control sub-population (n=3/genotype). (**G**, **N)** pKap1 expression in LT-HSCs was determined by intracellular flow cytometry analysis. Grey and open histograms represent isotype-matched control and pKap1 stains respectively. Unless stated, mean (SD) values are shown. *, P<0.05; **, P<0.005; ***, P<0.0005. The different BM hematopoietic

stem and progenitor populations were defined as follows: LT-HSC ($(L^-S^+K^+$ ($Lineage^-Sca\text{-}1^+cKit^+$) $CD34^{-/lo}Flt3^-$); ST-HSC ($L^-S^+K^+$ $CD34^+Flt3^-$); MPP ($L^-S^+K^+CD34^+Flt3^+$); CMP ($L^-S^-K^+IL7R^-CD34^+Fc\gamma R^-$); GMP (granulocyte-monocyte progenitor, $L^-S^-K^+IL7R^-CD34^+Fc\gamma R^+$); MEP (megakaryocytic-erythroid progenitor; $L^-S^-K^+IL7R^-CD34^-Fc\gamma R^-$); CLP ($L^-S^-K^{lo}IL7R^+$).

Figure 2. ATMIN-deficient mice have a reduced CMP compartment due to increased apoptosis. Black bars/symbols represent *Atmin*$^{f/f}$ and white Vav-*Atmin*$^{\Delta/\Delta}$ unless otherwise indicated. (**A**) DCFDA stains for ROS detection showing a mild increase in the percentage of ROS-positive cells in ATMIN-deficient CMPs (n=3/genotype). (**B**) Treating total BM cells with the antioxidants NAC or γ-GCE (not shown) was unable to rescue the myeloid colony formation (CFU) defect of Vav-*Atmin*$^{\Delta/\Delta}$ cells (n=5/genotype). (**C**) Expression of key anti-oxidant genes was unchanged between ATMIN-deficient and control CMPs. Expression values were determined by qRT-PCR and were relative to the mean (n=3-5/genotype). No significant increase in pKap1 levels (indicative of ATM activation) (**D**), upregulation of genes in the DNA oxidation repair pathway (**E**), or changes in the indicated CMP developmental factors (**F**) were detected in ATMIN-deficient compared to control CMPs. pKap1 levels were determined by intracellular flow cytometry analysis (MFI ratios are shown) and qRT-PCR was used to determine the expression of the indicated genes (n=5-6/genotype). (**G**) The frequency of late apoptosis was significantly increased and (**H**) *Dynll1* expression was drastically reduced in CMPs lacking ATMIN compared with control cells (n=4-6/genotype). (**I**) Representative cell images captured by an ImageStream flow cytometer in brightfield, followed by their respective composite images, showing higher co-localization of mitochondria (red) with Bim (green) staining in Vav-*Atmin*$^{\Delta/\Delta}$ CMPs. (**J**) Representative MitoTrackerRed-CMXRox and Bim similarity staining score histograms for *Atmin*$^{f/f}$ (black) and Vav-*Atmin*$^{\Delta/\Delta}$ (open)-derived CMPs respectively. A score above value 2 (R1) indicates translocation of Bim into mitochondria. (**K**) Percentage of Bim translocation in CMPs (n=3/genotype). Mean (SD) values are shown. $P<0.05$; ***, $P<0.0005$.

Figure 1

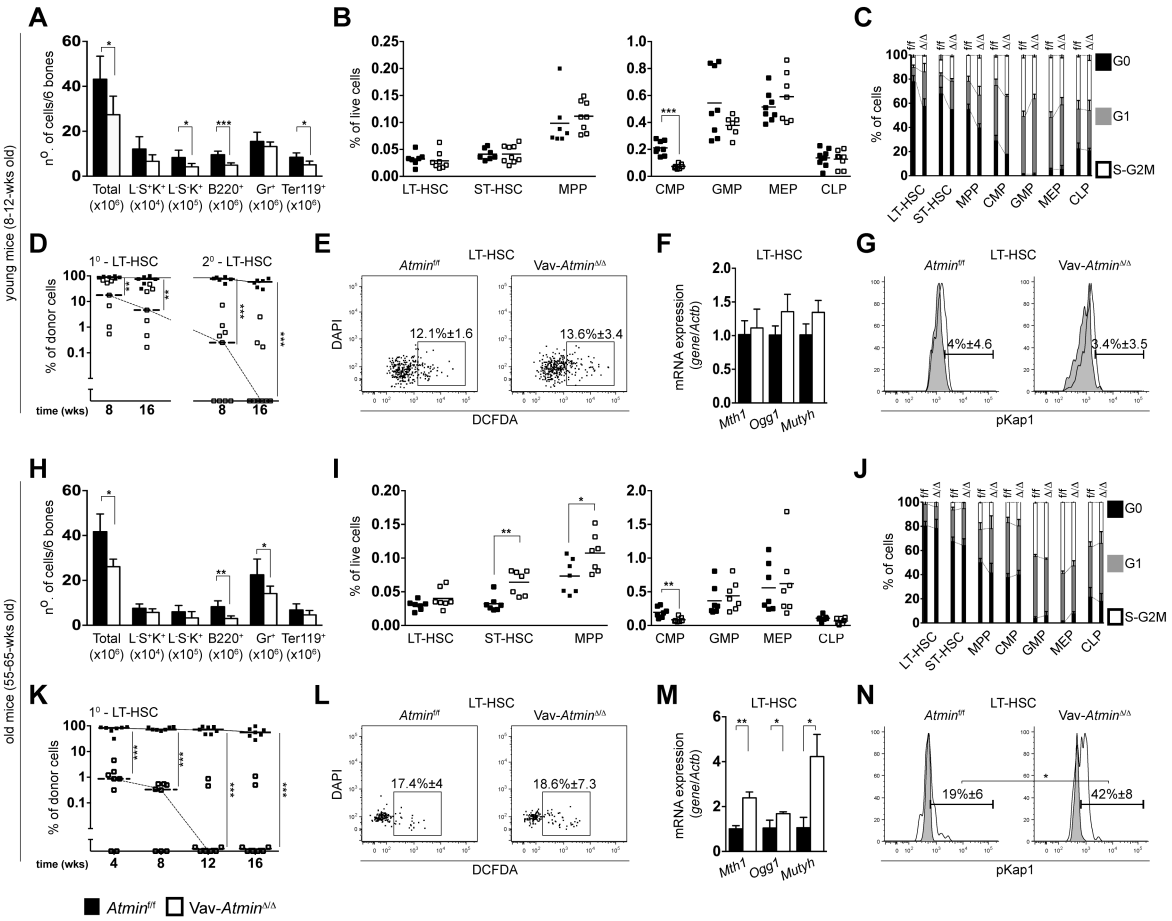
A
B
C
D
E
F
G
H
I
J
K
L
M
N
young mice (8-12-wks old)
old mice (55-65-wks old)
n°. of cells/6 bones
Total (x10⁶)
L⁻S⁺K⁺ (x10⁴)
L⁻S⁻K⁺ (x10⁵)
B220⁺ (x10⁶)
Gr⁺ (x10⁶)
Ter119⁺ (x10⁶)
% of live cells
LT-HSC
ST-HSC
MPP
CMP
GMP
MEP
CLP
% of cells
G0
G1
S-G2M
1° - LT-HSC
2° - LT-HSC
% of donor cells
time (wks)
Atmin f/f
Vav-Atmin Δ/Δ
DAPI
DCFDA
12.1%±1.6
13.6%±3.4
17.4%±4
18.6%±7.3
mRNA expression (gene/Actb)
Mth1
Ogg1
Mutyh
pKap1
4%±4.6
3.4%±3.5
19%±6
42%±8

Figure 2

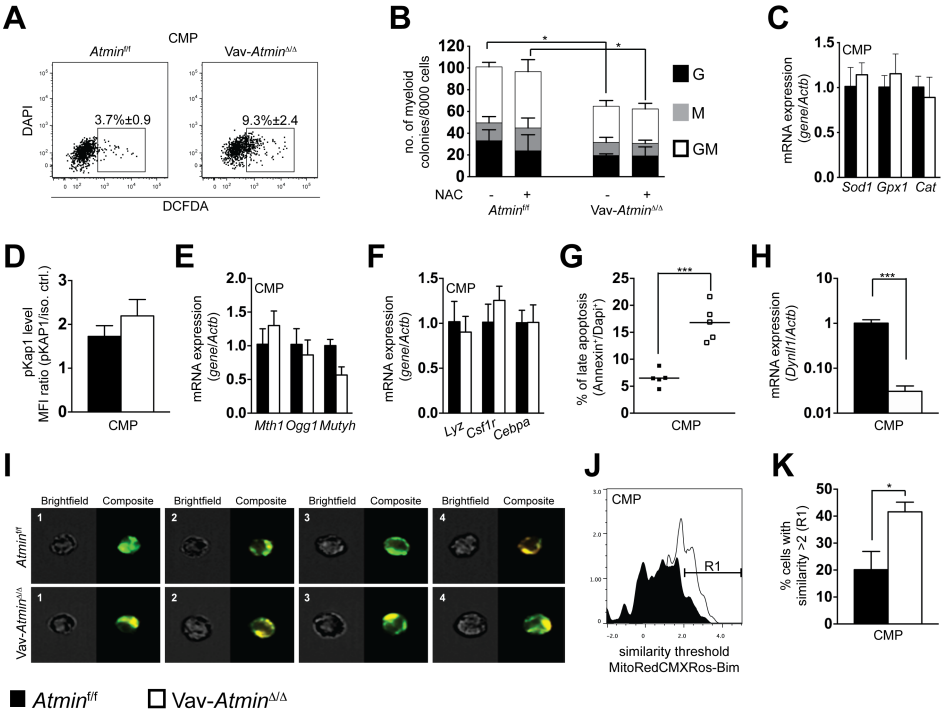
A
CMP
Atmin f/f
Vav-Atmin Δ/Δ
DAPI
3.7%±0.9
9.3%±2.4
DCFDA
B
no. of myeloid colonies/8000 cells
G
M
GM
NAC
Atmin f/f
Vav-Atmin Δ/Δ
C
CMP
mRNA expression (gene/Actb)
Sod1 Gpx1 Cat
D
pKap1 level MFI ratio (pKAP1/iso. ctrl.)
CMP
E
CMP
mRNA expression (gene/Actb)
Mth1 Ogg1 Mutyh
F
CMP
mRNA expression (gene/Actb)
Lyz Csf1r Cebpa
G
% of late apoptosis (Annexin+/Dapi-)
CMP
H
mRNA expression (Dynll1/Actb)
CMP
I
Brightfield
Composite
Atmin f/f
Vav-Atmin Δ/Δ
J
CMP
R1
similarity threshold MitoRedCMXRos-Bim
K
% cells with similarity >2 (R1)
CMP
Atmin f/f
Vav-Atmin Δ/Δ

Supplementary Figures

Figure S1. ATMIN-deficient mice are leukopenic. (**A**) Genotyping of *Atmin* WT, floxed and Δ alleles by PCR from tail, thymus, spleen and bone marrow (BM) of *Atmin*$^{f/f}$, *Atmin*$^{f/+}$ and Vav-*Atmin*$^{\Delta/\Delta}$ mice. (**B**) Representative western blot using *Atmin*$^{f/f}$ and Vav-*Atmin*$^{\Delta/\Delta}$ bone marrow lysates. Adult Vav-*Atmin*$^{\Delta/\Delta}$ mice are leukopenic but not anemic as shown by (**C**) the reduced absolute peripheral blood leukocyte (CD45^{+}), B cell, T cell, granulocyte and (**D**) red blood cell counts respectively (n=6/genotype; 8-12-wks old). Mean (SD) values are shown. *, P<0.05; ***, P<0.0005.

Figure S2. ATMIN-deficient mice have B cell lymphopenia. (**A**) Analysis of total B cell (B220^{+}) numbers in the spleens of Vav-*Atmin*$^{\Delta/\Delta}$ mice and *Atmin*$^{f/f}$ litter-mates (8-12-wk-old; n=5/genotype) showing a ~75% reduction in total B cell numbers in Vav-*Atmin*$^{\Delta/\Delta}$ mice compared with control mice. This was accompanied by a significant reduction in (**B**) the frequency of immature and re-circulating B cells (n=5/genotype) and (**C**) loss of germinal centre (GC) and red pulp regions (RP; representative H&E stainings of spleens are shown). (**D**) No increase in intracellular reactive oxygen species (ROS) was detected in the different Vav-*Atmin*$^{\Delta/\Delta}$ B cell sub-populations (n=3/genotype). (**E**) A significant 2-fold increase in early apoptosis was observed in all the different B cell sub-sets analyzed (each dot represents a mouse), likely caused by a Bim-dependent apoptotic mechanism[12] as a result of reduced *Dynll1* expression (a direct ATMIN transcriptional target[9]) detected in Vav-*Atmin*$^{\Delta/\Delta}$ cells (**F**). Expression values were determined by qRT-PCR and were relative to the mean of each control population (n=3-5/genotype). (**G**, **H**) *Atmin*-deleted B cells show an increase in pKap1 (an ATM substrate) and γH2AX compared with control B cells, indicating a higher DNA damage response in the absence of ATMIN. Expressions were determined by intracellular flow cytometry analysis and mean fluorescence intensity (MFI) ratios are shown. (**I**) Total B cell numbers are significantly reduced in the BM of Vav-*Atmin*$^{\Delta/\Delta}$ mice compared with *Atmin*$^{f/f}$ littermates (from two tibiae, two femurs and two iliac crests; n=6-7/genotype). Pre-B cell counts are reduced by 50%. (**J**) No accumulation of other primitive B cell sub-sets was observed in the absence

of ATMIN. (**K**) BM cells were unable to efficiently generate pre-B cell colonies *in vitro* (n=3/genotype; in triplicate each). Mean (SD) values are shown. *, P<0.05; **, P<0.005; ***, P<0.0005.

Figure S3. Defective regeneration capacity of Vav-*Atmin*$^{\Delta/\Delta}$ LT-HSCs after 5-FU treatment. (**A**) qRT-PCR for the expression of *Cdkn1c* and *Rbl2* in the indicated BM sub-populations. Expression values are relative to the mean of each control sub-population (n=3-5/genotype). Other cell cycle regulators were unchanged between ATMIN-deficient and control cells (data not shown). (**B**) Contribution of the transplanted primary LT-HSCs (as shown in Figure 1D) to the B, T and granulocyte cell lineages. Each symbol indicates a mouse and horizontal lines represent median reconstitution levels. (**C**) Frequency of late apoptosis in young LT-HSCs (n=4-6/genotype). (**D**) Kaplan-Meier survival curve of *Atmin*$^{f/f}$ and Vav-*Atmin*$^{\Delta/\Delta}$ mice injected 3 times (arrows) with 5-FU (n=6-8/genotype). Mean (SD) values are shown. *, P<0.05; **, P<0.005.

Supplementary Materials and Methods

Mice

NSG mice: Nonobese diabetic/severe combined immunodeficiency disease/interleukin-2 receptor γ-chain–null (NOD/SCID IL2Rγ^{null}; NSG) mice were originally obtained from Dr Leonard Schultz (Jackson Laboratory) and bred in the London Research Institute Biological Resources Unit. Mice were kept in micro-isolators and fed sterile food and acidified water. All experimental procedures were approved by London Research Institute ethics committees and conform to the UK Home Office regulations.

Bone marrow transplantation and 5-FU treatment

NSG mice aged 8 to 12 weeks were irradiated at 3.75 Gy (^{137}Cs source) up to 24 hours before tail vein injection of flow cytometry-purified primary cell populations. For secondary transplants, two NSG mice that received LT-HSCs from either *Atmin*$^{f/f}$ or Vav-*Atmin*$^{\Delta/\Delta}$ mice were randomly pooled and sorted again for LT-HSCs and injected into two sub-lethally irradiated NSG mice. Eight-twelve week-old *Atmin*$^{f/f}$ and Vav-*Atmin*$^{\Delta/\Delta}$ mice received 3-times injection of 5-FU (150 mg/Kg body weight) and were analyzed for different white blood cell counts and survival respectively.

Hematopoietic analyses

Single-cell suspensions were first obtained from different hematopoietic tissues, then red blood cells were lysed and samples stained for 30 min. at 4°C with the indicated antibodies in PBS supplemented with 2% FCS (PBS/2%). DAPI was added to exclude dead cells in the flow cytometry analysis. For complete blood counts, peripheral blood was collected from the tail vein into tubes containing K_2EDTA. Twenty-five μl of blood was stained for different leukocyte antigens as described then without washing diluted to 1 ml and analysed in a MACSQuant analyser (Miltenyi Biotec). For red blood cell counts, blood was diluted 1:1000 and red cells were counted in a hemocytometer. The following antibodies (from BD Bioscience and eBioscience) were used: Lineage cocktail, CD45.1 (A20), CD45.2 (104), B220 (RA3-6B2), Ly-6G (Gr1; RB6-8C5), CD3 (17A2), Sca-1 (D7), CD117 (c-Kit;

2B8), CD34 (RAM34), CD16/32 (93), CD43 (S7), IgM (II/41), CD135 (Flt3; A2F10), CD127 (IL7Rα; A7R34) and AnnexinV.

Analysis of intracellular ROS and mitochondria.

Cells were incubated with the ROS detection agent DCFDA (carboxy-H_2DFFDA C13293; Life Technologies) at 5 μM or MitoTrackerRed-CMXRos (M7512; Life Technologies) at 12.5 nM and incubated at 37°C for 30 min. After this period cells were washed with PBS/2% FBS containing trypan blue to quench nonspecific staining.

Gene Expression Analysis

RNA was extracted using the RNeasy Micro Kit (Qiagen, Inc.) and treated with DNase. Reverse transcription was performed using the SensiScript Kit (Qiagen) according to the manufacturer's instructions. For quantitative real-time polymerase chain reaction (qRT-PCR), SybrGreen master mix reagent (Applied BioSystems) was used and the amplification was done using the ABI Prism 7700 sequence detection system (Applied BioSystems). To avoid possible amplification of contaminating DNA and unprocessed mRNA, where possible, primers were designed to anneal the end parts of two exons. The specificity of the PCR products was verified by running a 2% agarose gel, in addition to using the dissociation curve software from the qRT-PCR system. Primers used are listed in Table S1.

Colony assays

Standard methylcellulose colony assay media, MethoCult® GF M3534 was used according to the manufacturer's instructions. NAC (N-acetyl cysteine; Sigma) or γ-GCE (glutathione monoethyl ester; Calbiochem) was added to the methylcellulose at 100 μM or 2 mM respectively when cells were seeded and then at day 5. Colonies were scored at day 10.

Immunohistochemistry and immunocytochemistry

Tissue was fixed overnight in 10% neutral buffered formalin, briefly washed with PBS and transferred into 70% ethanol, processed and

embedded into paraffin. Sections were cut at 4 μm for H&E staining and immunohistochemistry using an antibody against B220 (BD Biosciences) and pS139-γH2AX (Abcam). For cell suspensions cells were allowed to attach to poly-L-lysine coated slides for 15 min. Flow cytometry-purified sub-populations were sorted directly onto poly-L-lysine-coated slides containing PBS/2% FBS before fixation. All cells were fixed with 4% paraformaldehyde at RT for 10 min, permeabilized with PBS/0.1% TX for 10 min, blocked with 10% serum (donkey or goat) for 30 min at RT, incubated with primary antibodies at 4°C overnight and then with appropriate secondary antibodies for 1 hour at RT. Slides were mounted with Fluorescence Mounting Medium (Dako) containing DAPI for nuclear staining.

Western blotting

Cells were extracted in RIPA lysis buffer (NEB) supplemented with protease inhibitors (Sigma). Western blots were performed using standard procedures. Protein samples were separated by SDS–PAGE, and subsequently transferred onto nitrocellulose membranes. All primary antibodies were used at 1:1000 dilution and secondary antibodies at 1:2000. The following antibodies were used: p-S824-Kap1 (Bethyl Laboratories, Inc); ATMIN, (Millipore); β-actin (Sigma); α–tubulin (Abcam); HRP-conjugated goat anti-mouse/rabbit IgG (Sigma).

ImageStream analysis

Cells were stained first for extracellular antigens followed by mitochondria staining. Cells were then fixed, permeabilized and stained for Bim as described above. Samples were analyzed on an ASSIST calibrated Dual Camera, 12 Channel ImagestreamX Mark II Imaging Flow Cytometer (Amnis, Merck Millipore) using INSPIRE software (Amnis, Merck Millipore). Images were collected using a 60x objective lens and sample data were acquired on a low speed and high sensitivity setting. Fluorescence was measured from 405nm, 488nm and 642nm lasers. Laser powers were set to 30mW, 50mW and 30mW respectively. A dot-plot of area vs aspect ratio for Brightfield Ch01 was gated to exclude debris during data acquisition. Single

stained cells were measured and a compensation matrix created; the acquired data were compensated and analysed using IDEAS software (Amnis, Merck Millipore). Gates were set to include single, focused cells and then gated for cells which were dual stained with MitoTrackerRed-CMXRos (Ch04) and Bim AlexaFluor 488 (Ch02). The “similarity” feature was used to assess the colocalization of the MitotrackerRed-CMXRos and Bim on selected cell populations. The following modified feature and mask was used to measure and define the region where the colocalization of the 2 dyes occurs: Similarity Threshold: Similarity Threshold ((Object (M04, Ch04 MitoCMXRos, Tight), Ch04 MitoCMXRos: 60))_Ch02 Bim AF488_Ch04 MitoCMXRos. Cells which scored more than 2 on this feature were assessed to have high Bim/mitochondria colocalization.

Statistical analysis

T-tests were used for most analyses. Statistical analysis of the engraftment data was performed using the Mann-Whitney test. The P value for the Kaplan-Meier survival curve was calculated using the Mantel-Cox test.

Table S1. List of primers used in this study

GENOTYPING	FORWARD	REVERSE
Atmin Lox6133	5'-TCAGCATCTTCTCCAGAGAGACAG-3'	
Atmin Lox6617		5'-CACATGTGTACAGCACATTCATTG-3'
Atmin Lox10252		5'-CTCAGGGTACACATACTATGCTTGC-3'
Vav-cre	5'-AGATGCCAGGACATCAGGAACCTG-3'	5'-ATCAGCCACACCAGACACAGAGATC-3'

qRT-PCR	FORWARD	REVERSE
Cdkn1a (p21)	5'-GTGGCCTTGTCGCTGTCTT-3'	5'-GCGCTTGGAGTGATAGAAATCTG-3'
Cdkn1b (p27)	5'-TGGGTTAGCGGAGCAGTGT-3'	5'-TGTTCTGTTGGCCCTTTTGTT-3'
Cdkn1c (p57)	5'-CGCAAACGTCTGAGATGAGT-3'	5'-TCCGGTTCCTGCTACATGAA-3'
Cdkn2c (p18)	5'-GCAAAATAATGTAAACGTCAACG -3'	5'-AAATTGGGATTAGCACCTCTGAG-3'
Rbl2	5'-GCTCCTTACACGACGGTCTAGT-3'	5'-GCGGCTAACACGTATTCTTCA-3'
E2F4	5'-TGGCCTACGTGACTCATGAAG-3'	5'-TACTTCTTCTGGCCATTGAGAC-3'
Cdkn2a (p16Ink4a)	5'-AACTCTTTCGGTCGTACCCC-3'	5'-CGAATCTGCACCGTAGTTGAG-3'
Cdkn2a (p19Arf)	5'-GCTCTGGCTTTCGTGAACAT-3'	5'-CGAATCTGCACCGTAGTTGAG-3'
Dynll1	5'-CTCTGCTCCACGGTAACCAT-3'	5'-TGTTGTACTTCTCCAACGCC-3'
Lyz	5'-GGATATTTCAGATCAATAGCCGA-3'	5'-CACCCTCTTTGCACATTGTATG-3'
Csf1R	5'-AGCACCCTGACCACAAGAAAC-3'	5'-TGTGCCAGCAAATTCCAAGA-3'
Cebpa	5'-AACAGCAACGAGTACCGGGTA-3'	5'-TCATTGTCACTGGTCAACTCC-3'
Sod1	5'-GAGACCTGGGCAATGTGACT-3'	5'-CACCTTTGCCCAAGTCATCT-3'
Cat	5'-TGGCACACTTTGACAGAGAGC-3'	5'-CCTTTGCCTTGGAGTATCTGG-3'
Gpx1	5'-GATGAACGATCTGCAGAAGC-3'	5'- CGGACGTACTTGAGGGAATTC-3'
Mth1	5'-CAGGAAGGAGAGACCATTGAGA-3'	5'-GTCAGCCGAGAAGATATGCAC-3'
Ogg1	5'-CTAGCAGCATGAGACATCGC-3'	5'-ATACTTGATCTGCCAGCACG-3'
Mutyh	5'-GTATGACCAAGAGAAGCGTGAC-3'	5'-GCATAACCTCTGACACCCACAC-3'
Actb	5'-CTGTATTCCCCTCCATCGTG-3'	5'-CGTCCCAGTTGGTAACAATG-3'

Figure S1

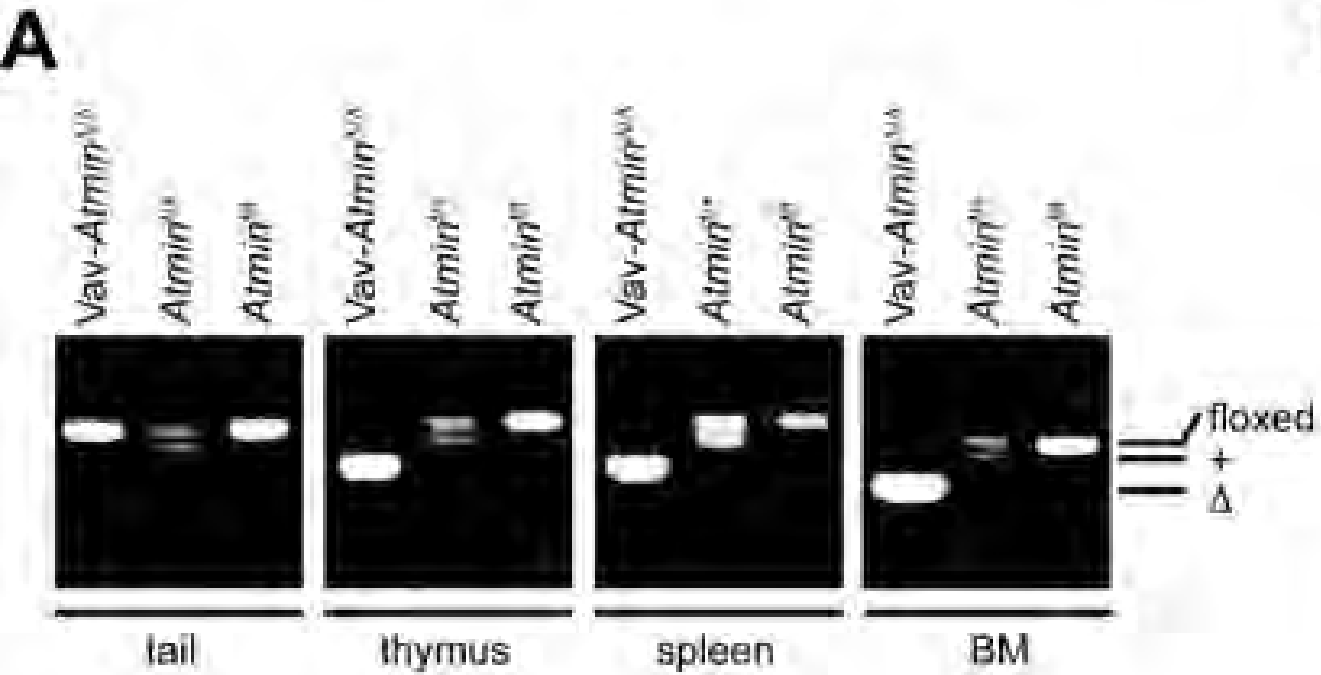
A
Vav-Atmin
Atmin
Atmin
floxed
+
Δ
tail
thymus
spleen
BM

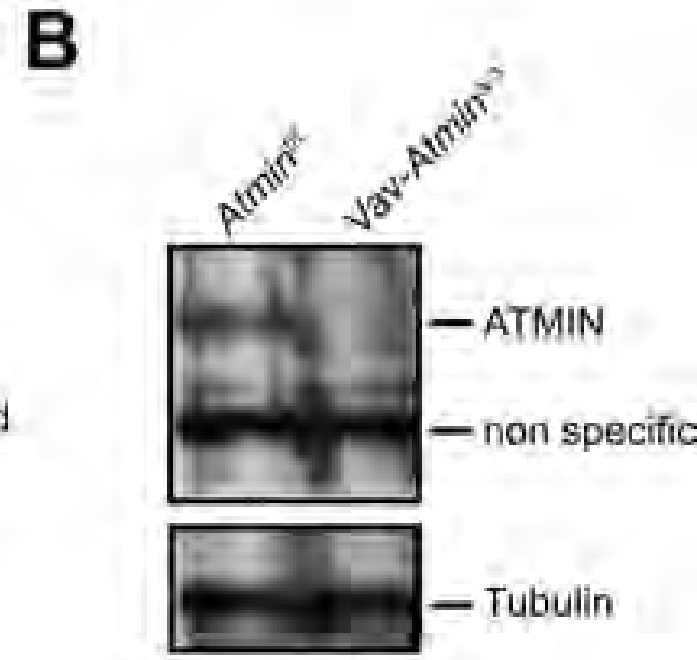
B
ATMIN
non specific
Tubulin

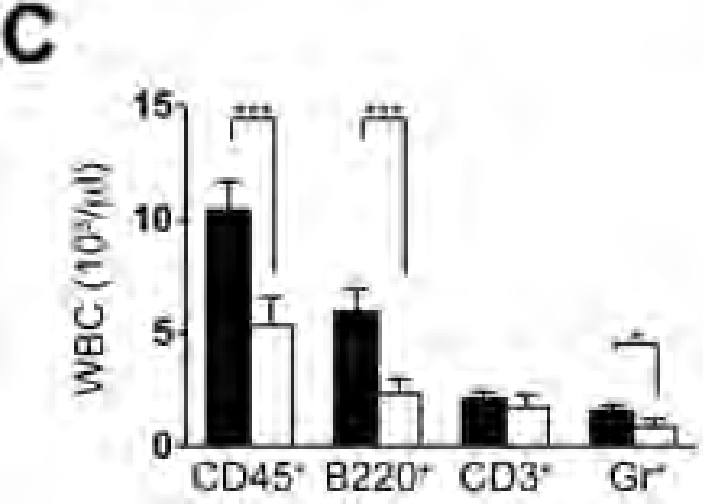
C
WBC (10³/μl)
15
10
5
0
***
***
*
CD45⁺
B220⁺
CD3⁺
Gr⁺

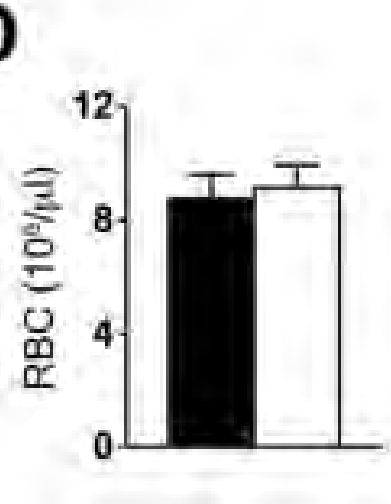
D
RBC (10⁶/μl)
12
8
4
0

Figure S2

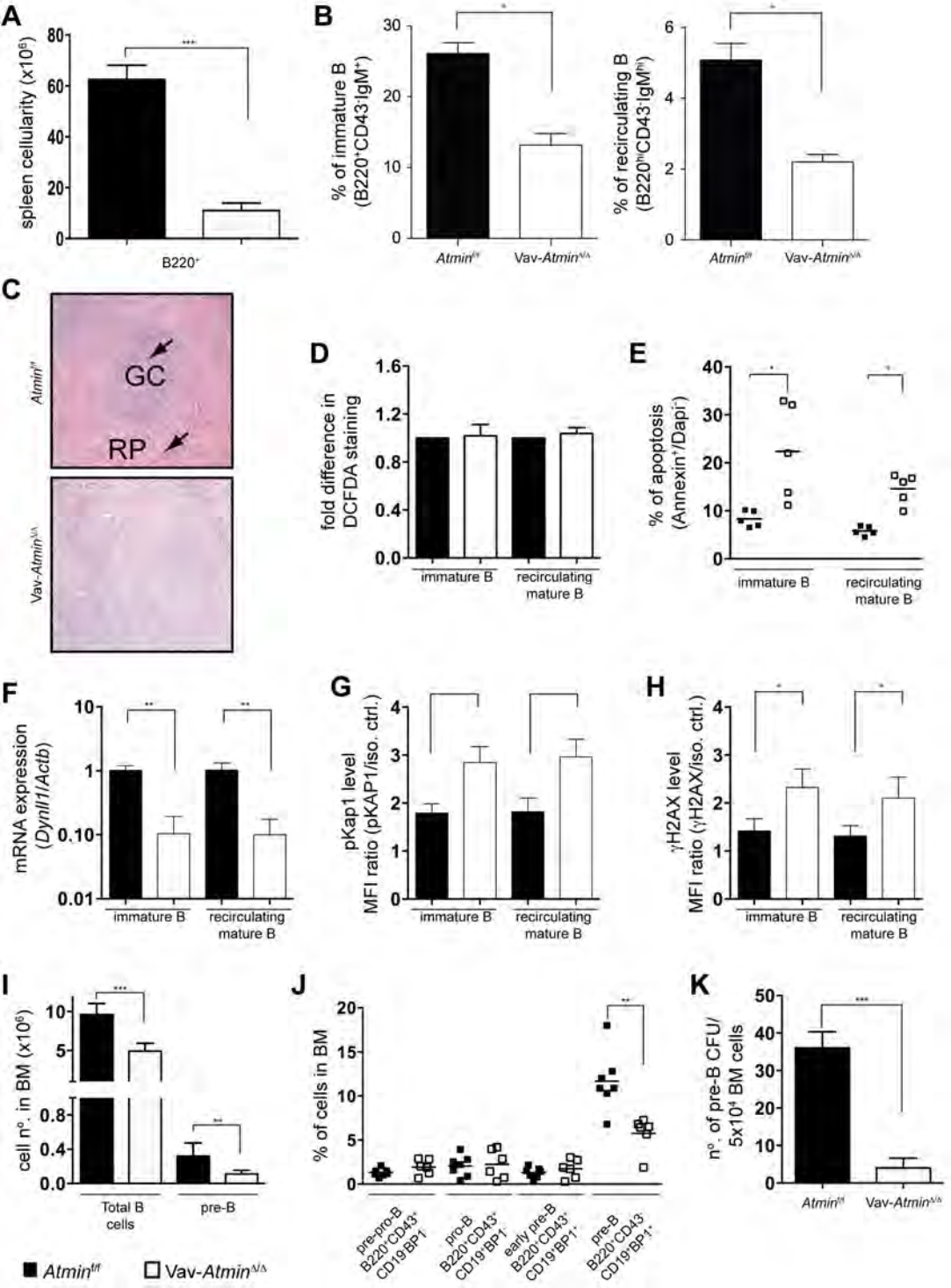
A
spleen cellularity (x10⁶)
B220⁺
B
% of immature B (B220⁺CD43⁻IgM⁺)
% of recirculating B (B220ʰⁱCD43⁻IgMˡᵒ)
Atmin^f/f
Vav-Atmin^Δ/Δ
C
GC
RP
Atmin^f/f
Vav-Atmin^Δ/Δ
D
fold difference in DCFDA staining
immature B
recirculating mature B
E
% of apoptosis (Annexin⁺/Dapi⁻)
immature B
recirculating mature B
F
mRNA expression (Dynll1/Actb)
immature B
recirculating mature B
G
pKap1 level MFI ratio (pKAP1/iso. ctrl.)
immature B
recirculating mature B
H
γH2AX level MFI ratio (γH2AX/iso. ctrl.)
immature B
recirculating mature B
I
cell n°. in BM (x10⁶)
Total B cells
pre-B
Atmin^f/f
Vav-Atmin^Δ/Δ
J
% of cells in BM
pre-pro-B B220⁺CD43⁺ CD19⁻BP1⁻
pro-B B220⁺CD43⁺ CD19⁺BP1⁻
early pre-B B220⁺CD43⁻ CD19⁺BP1⁺
pre-B B220⁺CD43⁻ CD19⁺BP1⁺
K
n°. of pre-B CFU/ 5x10⁴ BM cells
Atmin^f/f
Vav-Atmin^Δ/Δ

Figure S3

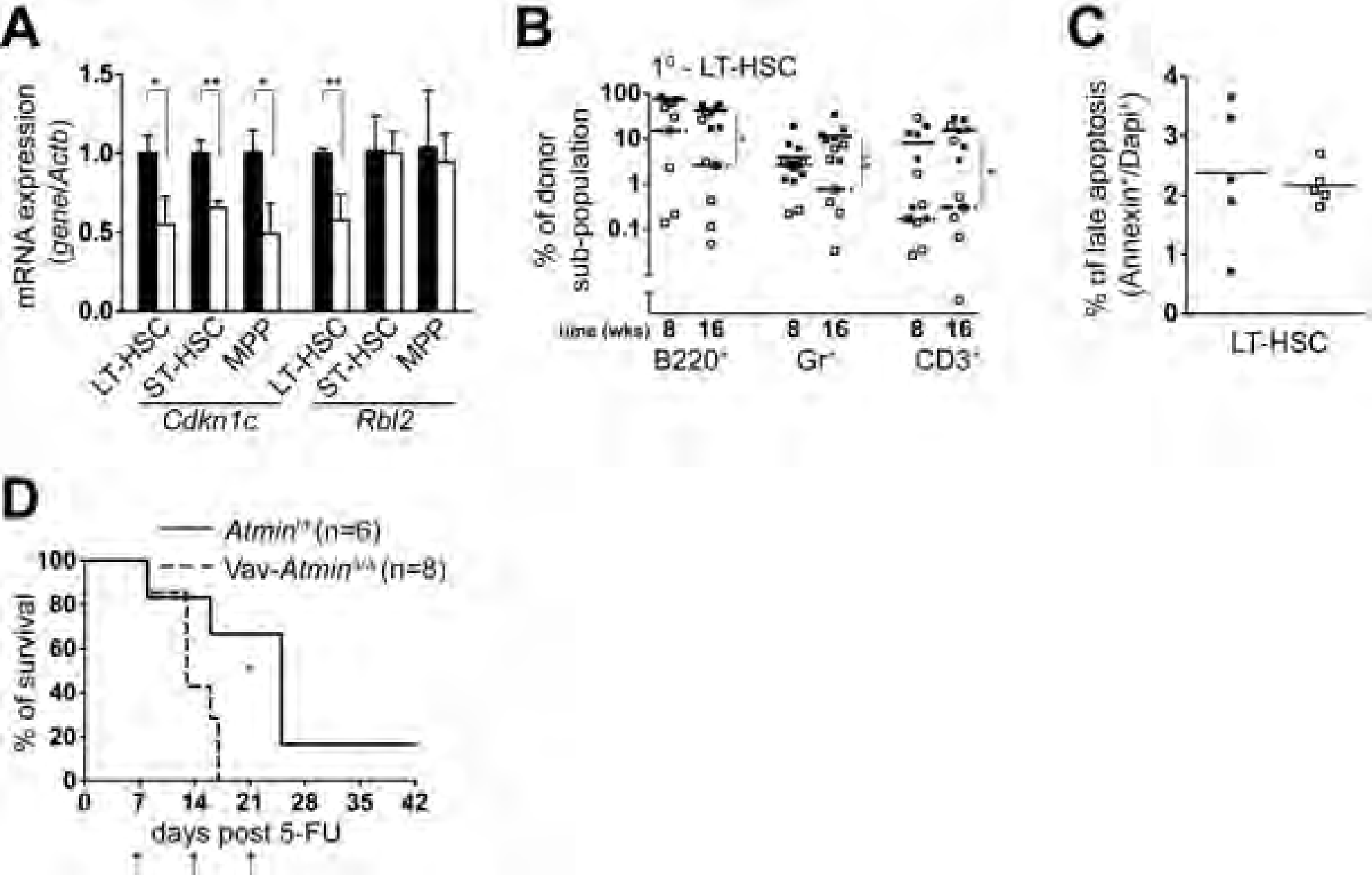
A
mRNA expression (gene/Actb)
1.5
1.0
0.5
0.0
LT-HSC
ST-HSC
MPP
LT-HSC
ST-HSC
MPP
Cdkn1c
Rbl2
B
1° - LT-HSC
% of donor sub-population
100
10
1
0.1
time (wks) 8 16 8 16 8 16
B220+
Gr+
CD3+
C
% of late apoptosis (Annexin+/Dapi-)
4
3
2
1
0
LT-HSC
D
Atmin+/+ (n=6)
Vav-Atmin Δ/Δ (n=8)
% of survival
100
80
60
40
20
0
0 7 14 21 28 35 42
days post 5-FU